Journal of Controlled Release 258 (2017) 43–55

Contents lists available at ScienceDirect

Journal of Controlled Release

journal homepage: www.elsevier.com/locate/jconrel

Doxorubicin delivered by a redox-responsive dasatinib-containing polymeric prodrug carrier for combination therapy

Jingjing Sun[a,1], Yanhua Liu[b,1], Yichao Chen[a], Wenchen Zhao[a], Qianyu Zhai[c], Sanjay Rathod[a], Yixian Huang[a], Suoqin Tang[c], Yong Tae Kwon[a,d], Christian Fernandez[a], Raman Venkataramanan[a], Song Li[a,*]

[a] Center for Pharmacogenetics, Department of Pharmaceutical Sciences, School of Pharmacy, University of Pittsburgh, Pittsburgh, PA 15261, United States
[b] Department of Pharmaceutics, School of Pharmacy, Ningxia Medical University, No. 1160, Shengli Street, Yinchuan 750004, China
[c] Department of Pediatrics, The General Hospital of People's Liberation Army, Beijing 100853, China
[d] Protein Metabolism Medical Research Center, Department of Biomedical Sciences, College of Medicine, Seoul National University, Seoul 110-799, Republic of Korea

ARTICLE INFO

Keywords:
Dasatinib
Prodrug micelles
Redox responsive
Doxorubicin
Co-delivery

ABSTRACT

Two novel prodrug polymers POEG-*b*-PSSDas (redox-sensitive) and POEG-*b*-PCCDas (redox-insensitive), which consist of poly(oligo(ethylene glycol) methacrylate) (POEG) hydrophilic blocks and dasatinib (DAS, an oncogenic tyrosine kinases inhibitor) conjugated hydrophobic blocks, were designed as dual-functional carriers for codelivery with doxorubicin (DOX). Both carriers retained antitumor activity of DAS and could form mixed micelles with DOX. Compared to POEG-*b*-PCCDas micelles, incorporation of disulfide linkage into POEG-*b*-PSSDas micelles facilitated efficient cleavage of DAS from prodrug micelles in tumor cells/tissues, leading to a higher level of anti-tumor activity in vitro and in vivo. In addition, DOX-loaded POEG-*b*-PSSDas micelles exhibited triggered DOX release under a redox environment (10 mM glutathione, GSH), and demonstrated enhanced cytotoxicity against 4T1.2 and PC3 cell lines compared to DOX and DOX-loaded POEG-*b*-PCCDas micelles. More importantly, DOX-loaded POEG-*b*-PSSDas micelles were more effective in inhibiting the tumor growth and prolonging the survival rate in an aggressive murine breast cancer model (4T1.2) compared to DOX-loaded POEG-*b*-PCCDas micelles and a micellar formulation co-loaded with DOX and DAS. This redox-responsive prodrug micellar system provides an attractive strategy for effective combination of tumor targeted therapy and traditional chemotherapy, which warrants further investigation.

1. Introduction

Owing to the intrinsic heterogeneity of tumor cells, monotherapy based on a single drug has some limitations in cancer treatment, such as drug resistance, narrow therapeutic windows and inevitable side effect induced by high dosage of single drug [1,2]. Combination therapy with multiple drugs of different anti-cancer mechanisms can overcome these limitations and thus becomes a promising strategy in clinical cancer treatments [3,4].

It is well known that the success of combination therapy greatly depends on the choice of drugs. Recently, the focus of drug screening has shifted from traditional chemotherapeutics to molecular targeted therapeutics, including monoclonal antibodies and small molecule inhibitors [5,6]. Different from traditional cytotoxic chemotherapy, targeted therapy inhibits the proliferation of cancer cells through interfering with specific signaling pathways and relevant kinases involved in the tumor development and metastasis. Dasatinib (DAS) is a FDA-approved multi-targeted inhibitor that targets to various critical oncogenic tyrosine kinases, including BCR/ABL kinases and Src family kinases (SFK) [7–10]. Encouraging outcomes have been obtained for DAS treatment in various cancers, such as leukemia, lung cancer, prostate cancer and ovarian cancer [11–13]. More importantly, DAS exhibits a reduced side effect compared with traditional cytotoxic chemotherapeutic drugs [14,15]. Because of its distinct anti-cancer mechanism and toxicity, DAS has become an excellent candidate for combination therapy with traditional chemotherapeutic drugs, including cisplatin [16], paclitaxel (PTX) [17–19] and doxorubicin (DOX) [20–22]. However, the extremely low solubility of DAS and different pharmacokinetic properties of the combined drugs will lead to poor uptake and suboptimal dose ratio of the two drugs at the tumor sites

* Corresponding author.
E-mail address: sol4@pitt.edu (S. Li).
[1] The two authors contributed equally. The manuscript was written through contributions of all authors. All authors have given approval to the final version of the manuscript.

http://dx.doi.org/10.1016/j.jconrel.2017.05.006
Received 2 December 2016; Received in revised form 25 April 2017; Accepted 5 May 2017

[23,24]. Besides, direct use of these drugs via systemic administration might result in poor biodistribution and severe systemic toxicities. As a result, it is highly demanded to develop safe and efficient delivery strategies which can co-deliver the two drugs to tumor sites to improve the therapeutic efficacy and minimize the systemic toxicities.

Over the past decades, polymers with diverse structures have been widely explored as drug delivery carriers [25–28]. Among them, micelles formed by amphiphilic polymers have attracted tremendous attention due to the capability of encapsulating hydrophobic drugs and efficient delivery of encapsulated drugs to tumor sites via the enhanced permeability and retention (EPR) effect [29]. For example, PEG-PCL polymeric micelles were employed as a carrier to encapsulate DAS, and it was found that DAS encapsulated in this carrier significantly inhibited the proliferation, adhesion and migration of tumor cells compared to free DAS, which might be attributable to the enhanced solubility of DAS [30]. Our group previously developed a PEG-Fmoc (PLFCL) micellar carrier for co-delivery of DAS and DOX, and DOX & DAS/PLFCL nanomicelles demonstrated improved synergistic anticancer activity compared to the combination of free DOX and DAS in vivo [31]. Nevertheless, these systems showed limited DAS loading capacity (< 4% wt) and relatively low stability, especially when co-encapsulating other drugs, which necessitates the use of a large amount of pharmacologically "inert" carriers to deliver sufficient dose of DAS to tumor tissues.

Alternatively, prodrug polymers provide an attractive strategy to increase the drug payload and reduce the amount of inert material [32,33]. Moreover, prodrug polymers with amphiphilic properties could be used as dual-functional carriers to co-load other drugs and achieve synergistic effect [34]. Furthermore, polymeric prodrug carriers can realize controlled release of both conjugated drugs and encapsulated drugs in response to a particular stimulus via introducing stimuli-responsive linkages between the drug and the polymer backbone. It is reported that the glutathione (GSH) concentrations (2–10 mM) in the cytoplasm are 100–1000 fold higher than that in the extracellular compartment. In addition, GSH levels are found to be further increased in tumor tissues compared to the normal tissues [35,36]. Therefore, disulfide linkages can be incorporated into the prodrug polymers to generate redox-responsive nanoparticles, which are able to promote drug release in the tumor cells [37,38].

In this work, we designed and synthesized a redox-responsive DAS-based prodrug polymer by introducing a disulfide linkage between DAS and polymer backbone, denoted as POEG-*b*-PSSDas. For comparison, POEG-*b*-PCCDas prodrug polymer without disulfide linkage was also synthesized (Scheme 1). These amphiphilic polymers could self-assemble to form prodrug micelles and serve as carriers to further encapsulate DOX. We hypothesize that DOX-loaded POEG-*b*-PSSDas micelles could rapidly release DOX and DAS following uptake by tumor cells as a result of disulfide cleavage under high redox environment, leading to effective therapy (Scheme 2).

2. Materials and methods

2.1. Materials

Dasatinib and DOX·HCl were purchased from LC Laboratories. 4-nitrophenyl chloroformate was purchased from Acros. 2-Azobis(isobutyronitrile) (AIBN) was purchased from Sigma-Aldrich and purified by recrystallization in anhydrous ethanol. Dulbecco's phosphate buffered saline (DPBS) was purchased from Lonza. Penicillin-streptomycin solution and fetal bovine serum (FBS) were purchased from Invitrogen. Dulbecco's Modified Eagle's Medium (DMEM), trypsin-EDTA solution, 3-(4,5-dimethylthiazol-2-*yl*)-2,5-diphenyl tetrazolium bromide (MTT), Triton X-100, Hoechst 33342 and LysoTracker Green DND-26 were all purchased from Sigma-Aldrich. *N*-methacryloyl-*N*-(*tert*-butoxycarbonyl)aminohexyl methacrylamide (MBA) [39], *N*-methacryloyl-*N*′-(*t*-butyoxycarbonyl)cystamine (MBC) [40], POEG macroCTA [34], and 4-nitrophenyl-actived dasatinib Das-NO_2 [41] were prepared according to the literatures. All other reagents were of analytical or chromatographic grade.

2.2. Synthesis of POEG-*b*-PMBA and POEG-*b*-PMBC polymers

AIBN (1 mg, 0.0062 mmol), POEG macroCTA (175 mg, 0.0194 mmol), MBA (128 mg, 0.45 mmol) or MBC monomer (144 mg, 0.45 mmol) and 1 mL dried 1,4-dioxane were added into a Schlenk tube, and deoxygenated by free-pump-thawing for three times. Then the mixture was filled with N_2 and immersed into an oil bath thermostated at 85 °C (for MBA monomer)/90 °C (for MBC monomer) to start the polymerization. After 24 h, the reaction was quenched by immersing the tube into liquid nitrogen and the mixture was precipitated in diethyl ether for 3 times. The POEG-*b*-PMBA and POEG-*b*-PMBC polymers were obtained after vacuum drying. Conversion of MBA monomer was 53% and conversion of MBC monomer was 50%.

^{1}H NMR of POEG-*b*-PMBA (400 MHz, $CDCl_3$): 4.12 (s, 4H), 3.67 (s, 60H), 3.40 (s, 6H), 3.10 (s, 4H), 2.10–1.62 (brm, 6H), 1.58–1.19 (brm, 20H), 1.15–0.76 (brm, 9H);

^{1}H NMR of POEG-*b*-PMBC (400 MHz, $CDCl_3$): 4.12 (s, 4H), 3.67 (s, 60H), 3.52–3.42 (m, 4H), 3.40 (s, 6H), 2.85 (s, 4H), 2.10–1.62 (brm, 6H), 1.44 (s, 10H), 1.15–0.76 (brm, 9H).

2.3. Synthesis of POEG-*b*-PCCDas and POEG-*b*-PSSDas polymers

The POEG-*b*-PMBA and POEG-*b*-PMBC polymers were deprotected at room temperature in TFA/DCM (1/1, v/v) mixture for 2 h, and then precipitated in cold diethyl ether and dried in vacuum to give the Boc-deprotected products POEG-*b*-PCC and POEG-*b*-PSS. Then, the as-synthesized Boc-deprotected polymers (130 mg, 0.011 mmol) and 4-nitrophenyl-actived dasatinib Das-NO_2 (220 mg, 0.337 mmol) were dissolved in 4 mL DMSO with 180 μL DIPEA. After stirring at 37 °C for 24 h, the reaction mixture was transferred into a dialysis bag (3500 Da MW cutoff) against DMSO for 2 days, and then deionized water for 1 day. The final products POEG-*b*-PCCDas and POEG-*b*-PSSDas were obtained after lyophilization.

^{1}H NMR of POEG-*b*-PCCDas (400 MHz, DMSO-d_6): 9.87 (s, 1H), 8.22 (s, 1H), 7.39–7.16 (brm, 3H), 4.10 (s, 4H), 3.52 (s, 60H), 3.26 (s, 6H), 3.10 (s, 4H), 2.10–1.62 (brm, 6H), 1.58–0.76 (brm, 15H);

^{1}H NMR of POEG-*b*-PSSDas (400 MHz, DMSO-d_6): 9.87 (s, 1H), 8.22 (s, 1H), 7.39–7.16 (brm, 3H), 4.10 (s, 4H), 3.52 (s, 60H), 3.46–3.39 (m, 4H), 3.26 (s, 6H), 2.85 (s, 4H), 2.10–1.62 (brm, 6H), 1.15–0.76 (brm, 9H).

2.4. Characterization of the synthesized monomer and polymers

^{1}H NMR spectrum was examined on a Varian-400 FT-NMR spectrometer at 400.0 MHz with $CDCl_3$ and DMSO-d_6 as the solvent. Molecular weight (M_n and M_w) and distribution (M_w/M_n) of the synthesized polymers were measured by gel permeation chromatography (GPC) performed on a Waters 515 HPLC pump and a Waters 717 Plus Autosampler equipped with a Waters 2414 refractive index detector. Tetrahydrofuran (THF) was used as the eluent with a flowing rate of 1.0 mL/min at 35 °C. A series of commercial polystyrene standards with narrow molecular weight distribution were applied to calibrate the GPC elution traces.

2.5. Preparation and characterization of blank and DOX-loaded micelles

Doxorubicin base (DOX), used for the preparation of micelles, was obtained by the reaction of Doxorubicin·HCl (DOX·HCl) with 1.5 M equivalents of triethylamine in DMSO for 24 h. The blank and DOX-loaded redox-sensitive POEG-*b*-PSSDas micelles and redox-non-sensitive POEG-*b*-PCCDas micelles were prepared through a dialysis method. Briefly, POEG-*b*-PSSDas and POEG-*b*-PCCDas polymers were dissolved

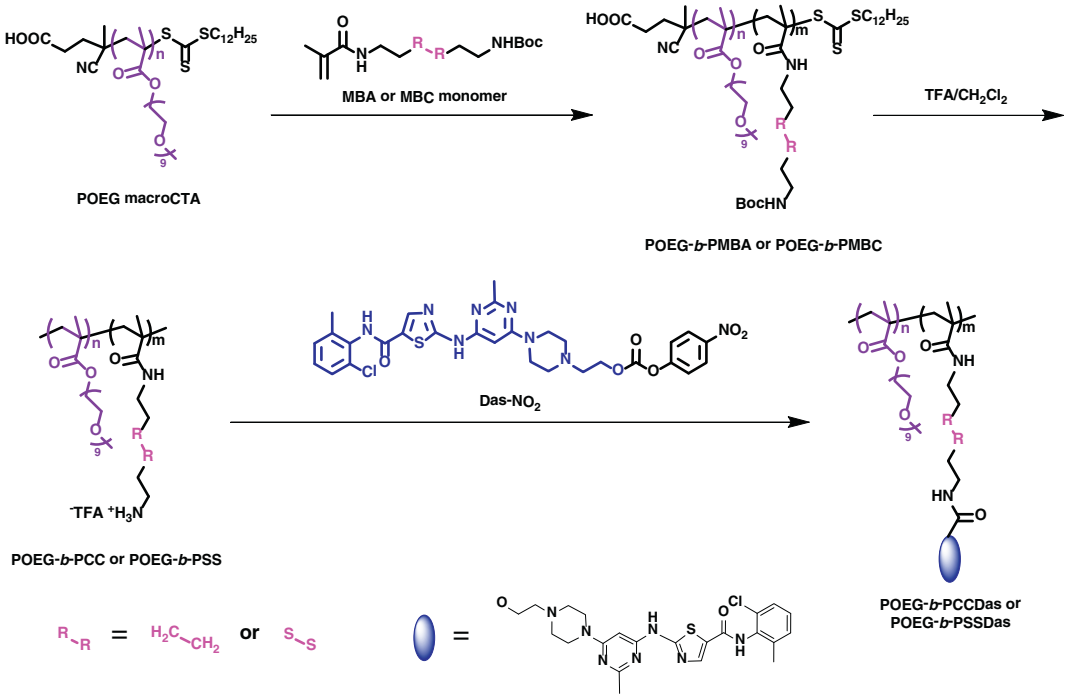

Scheme 1. Synthesis routes for POEG-*b*-PCCDas and POEG-*b*-PSSDas polymers via RAFT polymerization and post-modification.

in DMSO at a concentration of 10 mg/mL. DOX/DMSO stock solution (10 mg/mL) was added into the polymer solution (DOX/polymer = 10%, w/w) and the mixture was placed into a dialysis bag (MWCO 3.5 kDa), and dialyzed against 10 mM PBS for 3 days to remove free DOX and organic solvent. The solution was filtered through a 0.45 mm filter and then lyophilized. Blank micelles were similarly prepared except that no DOX was added.

The size distribution and zeta potential of blank and drug-loaded micelles were examined by dynamic light scattering (DLS) through a Malvern Zeta Nanosizer. The morphology was observed by transmission electron microscopy (TEM) using negative staining method.

The DOX concentration was detected by a Waters 2475 Fluorescence Detector with excitation at 490 nm and emission at 590 nm. The drug encapsulation efficiency (DEE) was calculated as

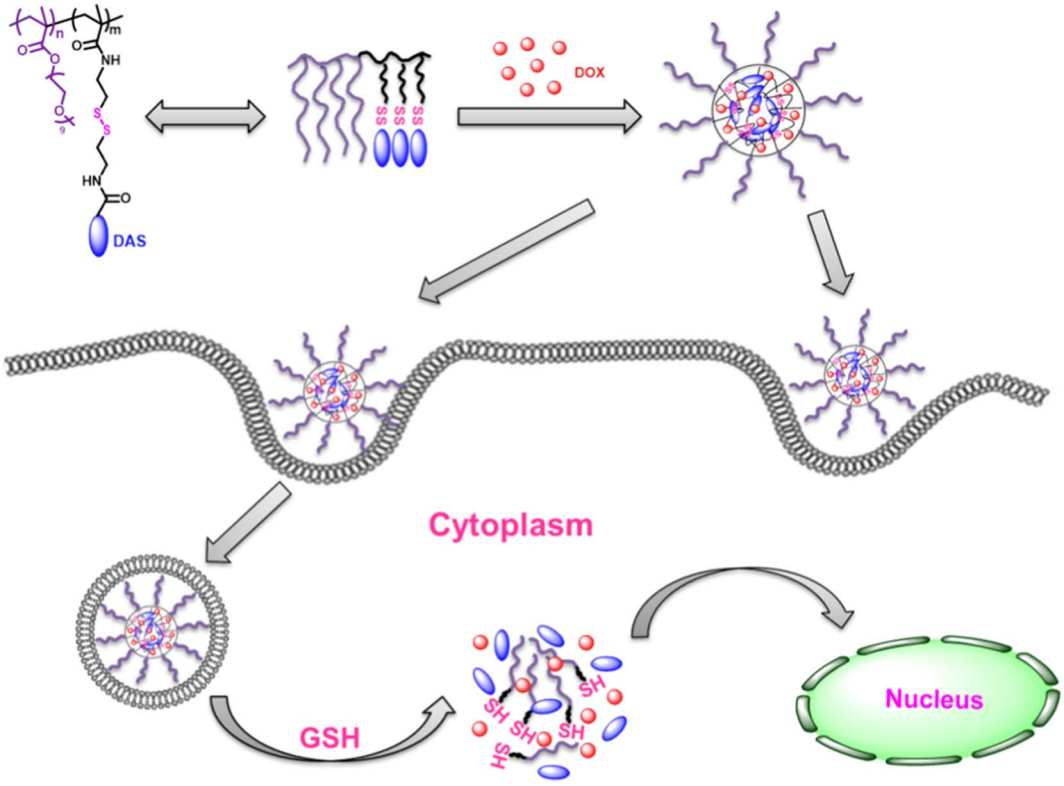

Scheme 2. Illustration of redox-sensitive POEG-*b*-PSSDas prodrug micelles as a carrier for co-delivery of DOX. This system can achieve controlled release of DAS and DOX in response to intracellular GSH.

the ratio between the amount of drug in the micelles and the amount of input drug. The drug loading capacity (DLC) was calculated as the percentage of the drug amount incorporated in the micelles versus the total amount of input materials (drug plus polymer).

2.6. Critical micelle concentration (CMC) of POEG-b-PFTS micelles

The CMC values of POEG-*b*-PCCDas and POEG-*b*-PSSDas micelles were determined by fluorescence measurement using nile red as a fluorescence probe. Briefly, nile red dissolved in DCM was added to test-tubes and the solvent was allowed to be evaporated at room temperature. POEG-*b*-PCCDas and POEG-*b*-PSSDas micelles ranging from 1.0×10^{-4} to 5×10^{-1} mg/mL were then added into nile red. The final concentration of nile red was kept at 6.0×10^{-7} M. The micelles were kept overnight to allow the solubilization equilibrium of nile red. Excitation was carried out at 550 nm and emission spectra were recorded from 570 to 720 nm. The CMC value was determined as the cross-point when extrapolating the intensity at low and high concentration regions.

2.7. Disassembly of blank micelles triggered by GSH

The disassembly of redox-sensitive POEG-*b*-PSSDas micelles in response to various concentrations of GSH was monitored by DLS to follow the size change at different time intervals. Briefly, 2 mL of POEG-*b*-PSSDas micellar solution containing GSH (10 μM and 10 mM) was placed in an incubation shaker at 37 °C at a rotation speed of 100 rpm for 4 h. For comparison, POEG-*b*-PSSDas micelles incubated without GSH and redox-non-sensitive POEG-*b*-PCCDas micelles with and without 10 mM GSH were included as controls, respectively.

2.8. In vitro DOX release in simulated extracellular and intracellular conditions

The DOX release from DOX/POEG-*b*-PSSDas and DOX/POEG-*b*-PCCDas micelles at various concentrations of GSH was studied using a dialysis method. Briefly, 2 mL of DOX/POEG-*b*-PSSDas micelles containing 0.5 mg of DOX were placed in a clamped dialysis bag (MWCO 3.5 kDa) and immersed in 80 mL of 0.1 M PBS buffer solution containing 0.5% (w/v) Tween 80 and various concentrations of GSH (0, 10 μM and 10 mM). The experiment was performed in an incubation shaker at 37 °C at 100 rpm. At selected time intervals, 4 mL aliquots of the medium were withdrawn and the same volume of fresh medium was added. For comparison, free DOX and DOX/POEG-*b*-PCCDas micelles incubated with and without 10 mM GSH were included as the redox-non-sensitive control. DOX release from micelles was measured by fluorescence spectrometry.

2.9. Cell culture

4T1.2 is a mouse metastatic breast cancer cell line. PC3 is a human prostate carcinoma cell line. The two types of cells were cultured in DMEM culture medium, containing 10% (v/v) fetal bovine serum and 100 IU/mL penicillin and 100 μg/mL streptomycin at 37 °C in a humidified 5% CO_2-95% air atmosphere.

2.10. Animals

Female BALB/c mice, 6–8 weeks in age, were purchased from Charles River (Davis, CA). All animals were housed under pathogen-free conditions according to AAALAC guidelines. All animal-related experiments were performed in full compliance with institutional guidelines and approved by the Animal Use and Care Administrative Advisory Committee at the University of Pittsburgh.

2.11. In vitro cytotoxicity assay

4T1.2 and PC3 cancer cell lines were used for in vitro cytotoxicity study. Cells were seeded in 96-well plates at a density of 1.5×10^3 (4T1.2) and 3×10^3 (PC3) cells/well and incubated 24 h to allow cell attachment. Then cells were treated with various concentrations of free DOX, DOX/POEG-*b*-PCCDas and DOX/POEG-*b*-PSSDas micelles. Other groups include cells treated with Das, blank POEG-*b*-PCCDas and POEG-*b*-PSSDas micelles at equivalent Das concentrations as in corresponding drug-loaded groups. After incubation for 72 h, the cell viability was measured via MTT assay as reported before [34]. Untreated cells were included as a control.

2.12. Cell uptake and intracellular trafficking

4T1.2 cells were seeded in glass bottom dishes (In Vitro Scientific, USA) at a density of 1×10^5 cells/dish. Following culture for 24 h, cells were treated with free DOX, DOX/POEG-*b*-PCCDas and DOX/POEG-*b*-PSSDas micelles in FBS-free culture medium (Life Technologies, USA) for 2 and 4 h, respectively. The concentration of DOX was kept at 20 μg/mL. Then cells were stained with Hoechst 33342 (1 mg/mL) for 20 min, and LysoTracker Green DND-26 (50 nM) (Invitrogen, USA) for 30 min, followed by three washes with ice-cold PBS. The intracellular distribution of DOX of various formulations was observed under a confocal laser scanning microscope (CLSM, FluoView 1000, Olympus, Japan).

2.13. Endocytosis pathways analyzed by flow cytometry (FCM)

4T1.2 cells were seeded into six-well plates at a density of 4.0×10^5 cells/well. Following culture for 24 h, cells were pre-incubated with three different endocytosis inhibitors separately for 30 min at the working concentrations that were not toxic to the cells (5 mM methyl-β-cyclodextrin (MBCD), 0.45 M sucrose, or 5 μM cytochalasin D) [42]. Then, the medium was replaced with fresh medium, and DOX/POEG-*b*-PCCDas and DOX/POEG-*b*-PSSDas micelles were added at a DOX concentration of 2 μg/mL, respectively. After incubation for 2 h, the culture medium was removed and the cells were washed twice with PBS. The cells were detached by trypsin, and the harvested cells were resuspended in 400 μL fresh medium for FCM assay. The mean fluorescence intensity of DOX in cells was analyzed in the FL2 channel by FCM (MACSQuant Analyzer 10, Miltenyi Biotec, Germany).

2.14. DAS release from POEG-b-PCCDas and POEG-b-PSSDas micelles

4T1.2 cells were seeded in a 6-well plate at a density of 3×10^5 cells/well. After 24 h of incubation for cell attachment, the medium was aspirated and the cells were incubated with blank POEG-*b*-PCCDas and POEG-*b*-PSSDas micelles for 24, 48 and 72 h. The cells were washed with ice-cold PBS three times and lysed with 0.1% Triton X-100. The lysates were vortexed and then centrifuged at 14,000 rpm for 10 min at 4 °C. Supernatants were subjected to MS analysis on a UPLC-QTOF MS system with an Acquity UPLC BEH C18 column. The amounts of DAS released from POEG-*b*-PCCDas and POEG-*b*-PSSDas micelles were presented as ng of DAS per microgram protein.

2.15. Plasma pharmacokinetics and tissue distribution

Female CD-1 mice (5 mice/group) were i.v. administered with DOX·HCl, DOX/POEG-*b*-PCCDas, and DOX/POEG-*b*-PSSDas micelles at a DOX dosage of 5 mg/kg. At different time points, blood samples were collected and centrifuged at 2500 rpm for 15 min. Acetonitrile (350 μL) was added to the plasma and the samples were centrifuged at 12,000 rpm for 5 min. Then, the supernatants were collected for HPLC analysis.

For tissue distribution study, female BALB/c bearing 4T1.2 tumors

(~400 mm^3) were used. DOX/POEG-*b*-PCCDas and DOX/POEG-*b*-PSSDas micelles were injected into the mice through tail vein at a dose of 5 mg DOX/kg body weight. One day post injection, mice were sacrificed and tumor tissues were collected, weighted and homogenized with 2 mL solvent (acetonitrile: H_2O = 1:1, v/v). The samples were centrifuged at 3500 rpm for 10 min, and the supernatants were collected and dried under airflow. The residues were then dissolved in a mixture of acetonitrile and H_2O (1:1, v/v) and centrifuged at 14,500 rpm for 10 min. The clear supernatants were collected for HPLC analysis.

2.16. In vivo therapeutic efficacy

Female BALB/c mice were s.c. inoculated with 4T1.2 cells at a density of 2×10^5 cells/mouse. When the tumor sizes reached around 50 mm^3, mice were randomly divided into six groups (n = 8) and i.v. administered with saline, DOX & Das/PEG-Fmoc micelles, blank POEG-*b*-PCCDas, blank POEG-*b*-PSSDas micelles, DOX/POEG-*b*-PCCDas and DOX/POEG-*b*-PSSDas micelles at a DOX dose of 5 mg/kg on days 0, 3 and 6, respectively. Tumor volumes were calculated according to the formula: $(L \times W^2) / 2$, in which L is the longest and W is the shortest tumor diameter (mm). Data were presented as relative tumor volume (the tumor volume at a given time point divided by the tumor volume prior to first treatment). Changes in body weights of all mice were also monitored during the entire course of treatment.

After completion of the in vivo therapy study, tumor tissues were excised and fixed in PBS solution containing 10% formaldehyde, followed by embedment in paraffin. The paraffin-embedded tumor samples were sectioned into slices at 5 μm using an HM 325 Rotary Microtome. The slices were then stained with hematoxylin and eosin (H & E) for histopathological examination under a Zeiss Axiostar plus Microscope (PA, USA).

In a separate experiment, the survival of the tumor-bearing mice was examined. The end point of survival was defined as animal death or when the implanted tumor volume reached ~1000 mm^3. The survival rate was plotted as Kaplan Meier curves and the median survival of mice was calculated.

2.17. Statistical analysis

Statistical analysis was performed with two-tailed Student's *t*-test between two groups and one-way analysis of variance (ANOVA) for multiple groups, followed by Newman-Keuls test if $p < 0.05$. Survival data were generated by the Kaplan-Meier method and statistical significance was determined by Mann Whitney U tests. In all statistical analyses, $p < 0.05$ was considered statistically significant, and $p < 0.01$ was considered highly statistically significant.

3. Results and discussion

3.1. Synthesis and characterization of POEG-b-PCCDas and POEG-b-PSSDas polymers

The POEG-*b*-PCCDas and POEG-*b*-PSSDas polymers were synthesized following Scheme 1. First, POEG macroCTA (M_n = 9 kDa, n = 18) was synthesized by reversible addition-fragmentation transfer (RAFT) polymerization as reported previously with some modification [34]. By using POEG macroCTA as RAFT chain transfer agent, MBA and MBC monomers were polymerized respectively to yield POEG-*b*-PMBA and POEG-*b*-PMBC polymers, and the polymerization kinetics was studied. As shown in Fig. S1A, the synthesis of POEG-*b*-PMBA diblock copolymer proceeded rapidly in 1, 4-dioxane at 85 °C without an obvious induction period. Fig. S1B depicts the kinetic plots of ln ($[M_0]/[M_t]$) versus reaction time, where $[M_0]$ denotes the initial monomer concentration and $[M_t]$ denotes the monomer concentration during polymerization. It exhibited a good linear relationship, indicating the living polymerization of MBA monomer. The polymerization of MBC monomer by POEG macroCTA proceeded very slowly at 85 °C with only 30% conversion being achieved after 24 h (data not shown). So we increased the polymerization temperature to 90 °C. Fig. S2 depicts the kinetic results of the plots for the synthesis of POEG-*b*-PMBC diblock copolymer. The polymerization rate was fast and around 53% conversion was obtained after 6 h (Fig. S2A). In the initial stage, the polymerization exhibited a linear relationship for the ln($[M_0]/[M_t]$) against time, indicating the living polymerization of MBC monomer (Fig. S2B).

The polymer structures of POEG-*b*-PMBA and POEG-*b*-PMBC were confirmed by ^1H NMR (Fig. S3). The peaks at 3.40 ppm (a) and 3.67 ppm (b, c) were attributed to the hydrophilic POEG block of the polymers. The peaks at 1.44 ppm were ascribed to the Boc groups of POEG-*b*-PMBA (f in Fig. S3A) and POEG-*b*-PMBC (h in Fig. S3B) respectively. The number of repeat units in the PMBA and PMBC blocks was calculated to be 9 based on the relative intensity ratio of the peaks at 3.40 ppm and 1.44 ppm. GPC analyses further confirmed the successful synthesis of POEG-*b*-PMBA and POEG-*b*-PMBC polymers (Table S1).

In the next step, the Boc-groups of the as-synthesized POEG-*b*-PMBA and POEG-*b*-PMBC polymers were deprotected in TFA/DCM solution. After deprotection, amine-bearing polymers POEG-*b*-PCC and POEG-*b*-PSS were obtained and characterized by ^1H NMR (Fig. S4). The peak at 1.44 ppm belonging to Boc group disappeared, which indicated the successful deprotection of Boc-groups.

4-nitrophenyl-actived dasatinib Das-NO_2 was synthesized according to the literature [41] and then conjugated with the POEG-*b*-PCC and POEG-*b*-PSS polymers to afford the POEG-*b*-PCCDas and POEG-*b*-PSSDas polymers, respectively. The structures of these polymers were characterized by ^1H NMR. As shown in Fig. 1, the successful conjugation of DAS to the polymers was confirmed by the appearance of peaks at 9.87 ppm, 8.22 ppm, 7.39–7.16 ppm and 6.06 ppm. By comparing the integrals of signals at 8.22 ppm (e) with those at 3.26 ppm (a), the number of DAS units per molecule was calculated to be 9, which indicated that almost all of the amine groups in the polymers were functionalized with DAS. DAS loading content in the POEG-*b*-PCCDas and POEG-*b*-PSSDas polymeric prodrug carriers is calculated to be around 28% (w/w) (Table 1), which is significantly higher than that of previously reported PEG-Fmoc carrier (4%) [31].

3.2. Physicochemical characterization of blank and DOX-loaded micelles

POEG-*b*-PCCDas and POEG-*b*-PSSDas prodrug micelles were prepared by a dialysis method. The CMC values of both prodrug micelles were measured by using nile red as a fluorescence probe. As shown in Fig. S5 and Table 1, POEG-*b*-PSSDas micelles showed decreased CMC values (13.2 μg/mL) compared to POEG-*b*-PCCDas micelles (21.3 μg/mL). The redox-sensitivity of POEG-*b*-PSSDas micelles was examined by monitoring the size changes in response to GSH with POEG-*b*-PCCDas micelles as a control (Fig. 2). It can be seen that the POEG-*b*-PCCDas micelles were stable in the presence of 10 mM GSH (Fig. 2A), while the size of POEG-*b*-PSSDas micelles increased from 167 to 1608 nm after exposure to 10 mM GSH for 4 h (Fig. 2B), indicating the partial disassembly of POEG-*b*-PSSDas micelles. We also evaluated the stability of the POEG-*b*-PSSDas micelles under 10 μM GSH which mimics the redox environment of the extracellular compartment. As shown in Fig. 2B, no obvious size change was observed for POEG-*b*-PSSDas micelles after 4 h incubation with 10 μM GSH, suggesting that POEG-*b*-PSSDas micelles could maintain its stability under the mildly redox environment in the blood circulation.

It has been reported that DAS synergizes with DOX to block cell growth, migration and invasion in a variety of breast cancer cell lines, and the synergy comes from inhibition of distinct pathways by DAS and DOX [21]. Our group further confirmed the synergistic effect of DAS and DOX in 4T1.2 breast cancer-bearing mice [31]. Therefore DOX was

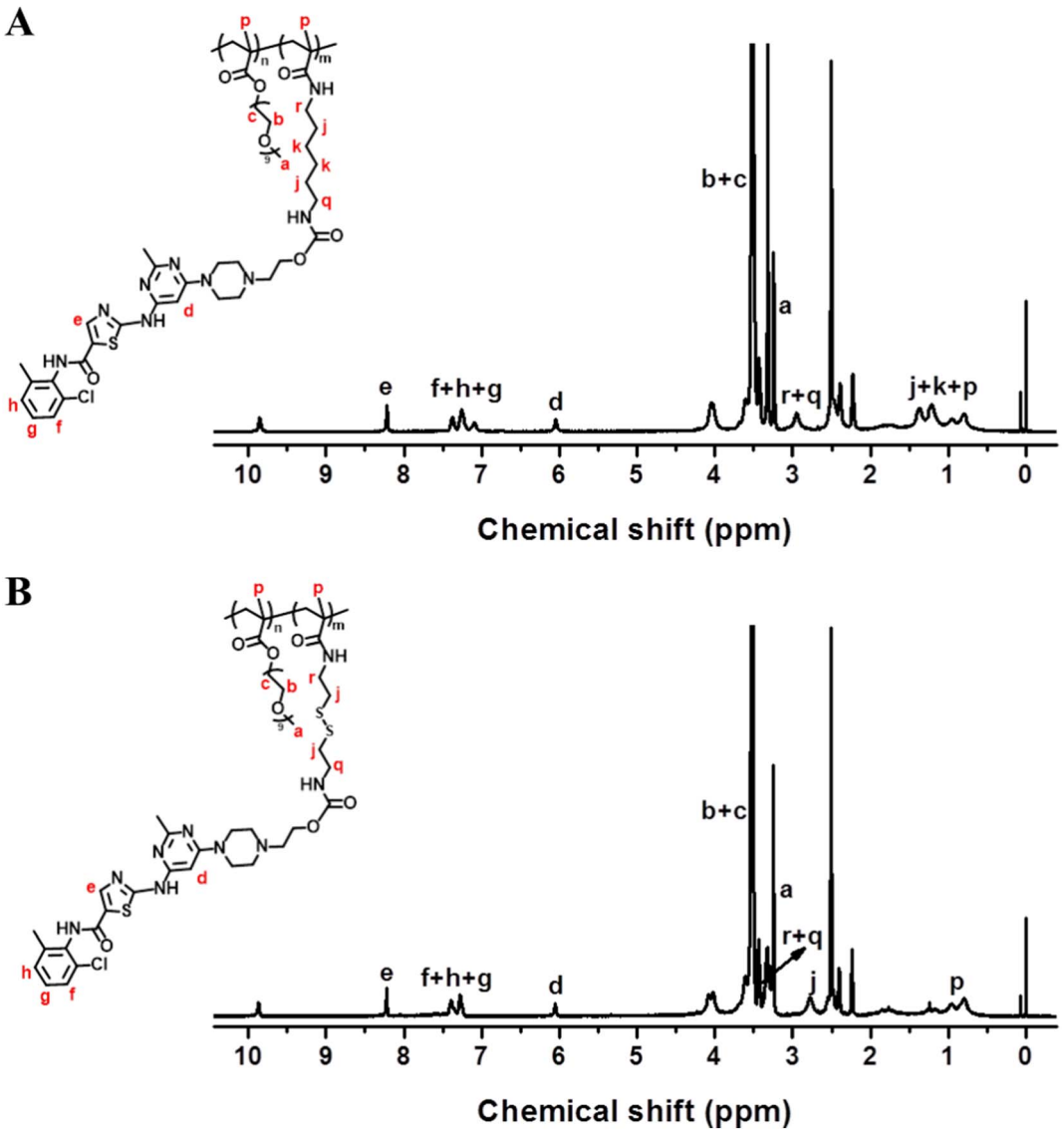

Fig. 1. ^{1}H NMR spectra of the $POEG_{18}$-*b*-$PCCDas_{9}$ (A) and $POEG_{18}$-*b*-$PSSDas_{9}$ (B) polymers in DMSO-d_6.

selected in this work as a model drug to evaluate the capability of POEG-*b*-PCCDas and POEG-*b*-PSSDas prodrug micelles as dual-functional carriers to achieve co-delivery of two different therapeutics. DOX-loaded micelles were similarly prepared as prodrug micelles, and DOX loading capacity and loading efficiency were examined by fluorescence measurement. As shown in Table 1, both POEG-*b*-PCCDas and POEG-*b*-PSSDas showed high DOX loading capacity (≥ 8.3%) and loading efficiency (≥ 90.0%). The size distribution and morphologies of both DOX-loaded micelles were characterized by DLS and TEM (Fig. 3). DOX-loaded POEG-*b*-PCCDas (Fig. 3A) and POEG-*b*-PSSDas (Fig. 3B) micelles showed an average hydrodynamic diameter of 187.9 nm and 200.8 nm, respectively, which were slightly larger than that of DOX-free micelles. The TEM images shown in Fig. 3C & D presented a spherical morphology for DOX-loaded POEG-*b*-PCCDas and POEG-*b*-PSSDas micelles. Fig. 3E & F show the particle size histograms obtained from the TEM data. The particle sizes of DOX-loaded POEG-*b*-PCCDas

Table 1
Physicochemical characterization of blank and DOX-loaded POEG-*b*-PCCDas and POEG-*b*-PSSDas micelles.

Micelles	Number of DAS units[a]	DAS content (%)[a]	Mass ratio (mg:mg)[b]	CMC (μg/mL)[c]	Size (nm)[d]	Zeta Potential (mV)[d]	DLC(%)[e]	DLE(%)[f]
POEG-*b*-PCCDas	9	28%	–	21.3	152.0	0.62	–	–
DOX/POEG-*b*-PCCDas	–		10:1	–	187.9	− 1.88	8.8	96.2
POEG-*b*-PSSDas	9	28%	–	13.2	167.6	− 1.56	–	–
DOX/POEG-*b*-PSSDas	–		10:1	–	200.8	− 1.32	8.3	90.0

[a] Calculated according to ^{1}H NMR results.
[b] CMC = critical micelle concentration.
[c] Mass ratio of the input polymer to DOX.
[d] Measured by dynamic light scattering particle sizer.
[e] DLC = DOX loading capacity.
[f] DLE = DOX loading efficiency.

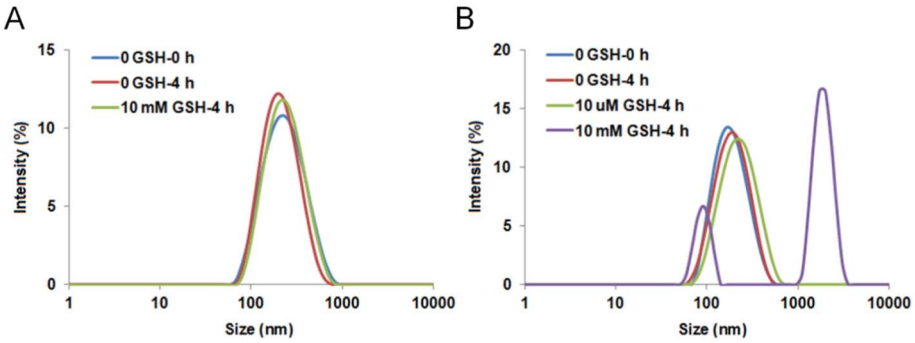

Fig. 2. Size change profiles of POEG-*b*-PCCDas (A) and POEG-*b*-PSSDas (B) micelles in response to GSH.

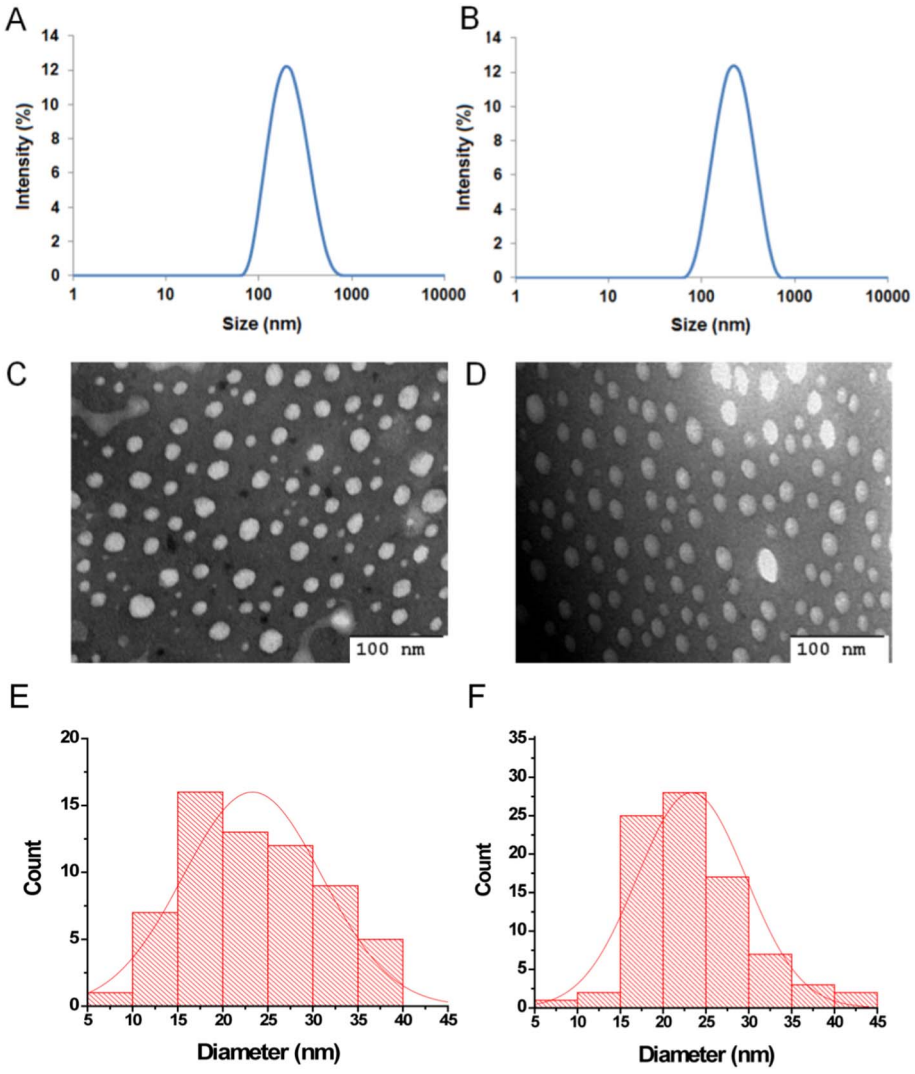

Fig. 3. The DLS measurements and TEM images of DOX-loaded POEG-*b*-PCCDas (A & C) and POEG-*b*-PSSDas (B & D) micelles. Scale bar is 100 nm. The size distribution histograms of DOX-loaded POEG-*b*-PCCDas (E, 23.1 ± 2.6 nm) and POEG-*b*-PSSDas (F, 23.7 ± 1.5 nm) micelles as determined from the TEM images.

and POEG-*b*-PSSDas micelles were determined to be 23.1 ± 2.6 nm (Fig. 3E) and 23.7 ± 1.5 nm (Fig. 3F), respectively. The difference in micelle sizes between the DLS and TEM might stem from the different principles of analysis involved in the two techniques [43]. DLS is an intensity-based technique, which is more sensitive to the larger particles. While TEM measurement is based on a scattering of electrons in sample irradiation, and shows stronger emphasis of the smallest components in the size distribution. Another possible reason is that DLS provides hydrodynamic size which includes the hydration layer around the particle, while TEM presents the size of the dried particle [44,45]. The zeta potentials of the blank and DOX-loaded micelles were also determined by the Zetasizer. As shown in Table 1, all of the micelles showed the zeta potentials close to 0 mV.

In vitro DAS and DOX release profiles were studied in PBS solution with varying GSH concentrations (0, 10 μM, 10 mM). As shown in Fig. 4A, little DAS release was observed from POEG-*b*-PCCDas micelles within 48 h in both the absence and presence of 10 mM GSH. For POEG-*b*-PSSDas micelles, little DAS was released in the presence of 10 μM

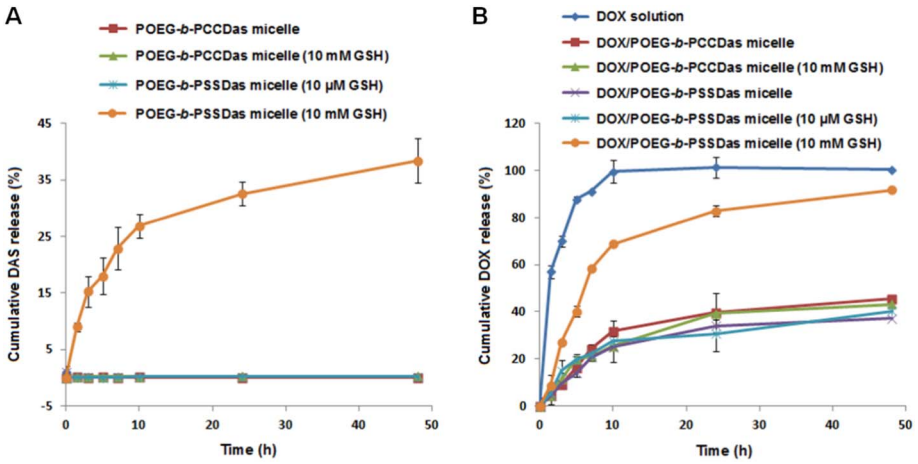

Fig. 4. (A) Cumulative DAS release profiles from POEG-*b*-PCCDas and POEG-*b*-PSSDas micelles. (B) DOX release profiles of DOX-loaded POEG-*b*-PCCDas and POEG-*b*-PSSDas micelles with free DOX as the control. PBS containing 0.5% (w/v) Tween 80 and different concentrations of GSH (0, 10 μM, 10 mM) was used as the release medium. Data are presented as means ± SD (n = 3).

GSH, further indicating the excellent stability of POEG-*b*-PSSDas micelles in the mildly redox environment of extracellular compartment, which was consistent with the result shown in Fig. 2B. In the presence of 10 mM GSH, the release of DAS from POEG-*b*-PSSDas micelles was accelerated with about 40% of DAS being released within 48 h.

DOX release profiles of DOX-loaded POEG-*b*-PCCDas and POEG-*b*-PSSDas micelles were shown in Fig. 4B. Free DOX solution showed burst release of DOX at pH 7.4, and almost 100% DOX was released at 12 h. In comparison, DOX-loaded POEG-*b*-PCCDas and POEG-*b*-PSSDas micelles showed a slow release of DOX in the absence of GSH, and only 30% of the total DOX was released at 12 h. In the presence of 10 mM GSH, no acceleration in DOX release was observed for DOX/POEG-*b*-PCCDas micelles, while DOX release from POEG-*b*-PSSDas micelles was drastically accelerated with 70% DOX being released after 12 h. This is likely due to the disassembly of micelles induced by GSH. We also noticed that addition of 10 μM GSH did not affect the release kinetics of DOX-loaded POEG-*b*-PSSDas. These results suggested that DOX-loaded POEG-*b*-PSSDas micelles are stable in the mildly redox environment of extracellular compartment, but are triggered to release DOX rapidly in response to highly redox environment after intracellular uptake.

3.3. In vitro cytotoxicity

The cytotoxicity of POEG-*b*-PCCDas and POEG-*b*-PSSDas prodrug micelles was examined by MTT assay in 4T1.2 and PC3 cells with free DAS as a control. As shown in Fig. 5, all the treatments inhibited the tumor cell proliferation in a DAS concentration dependent manner. Both POEG-*b*-PCCDas and POEG-*b*-PSSDas prodrug micelles exhibited lower cytotoxicity compared to free DAS at equivalent amounts of DAS, which suggested that not all of the DAS could be cleaved from the prodrug micelles in a relative short period of treatment. POEG-*b*-PSSDas prodrug micelles were more active in inhibiting tumor cell proliferation than POEG-*b*-PCCDas prodrug micelles in both 4T1.2 and PC3 tumor cells (Fig. 5A, B). The IC_{50} (half maximal inhibitory concentration) values of POEG-*b*-PCCDas and POEG-*b*-PSSDas in 4T1.2 and PC3 cells were summarized in Table S2. POEG-*b*-PSSDas showed IC_{50} values of 1.49 μg/mL and 2.34 μg/mL in 4T1.2 and PC3 cells respectively, which was much lower than those of POEG-*b*-PCCDas (4.79 μg/mL in 4T1.2 cells and 13.9 μg/mL in PC3 cells). The enhanced cytotoxicity of POEG-*b*-PSSDas may be attributed to the improved release of DAS from the prodrug micelles through the GSH-mediated cleavage of disulfide linkage in the cytoplasm.

To test this hypothesis, the concentrations of released DAS in 4T1.2 cells were analyzed by HPLC-MS at different time points (24 h, 48 h, 72 h) following treatment with POEG-*b*-PCCDas or POEG-*b*-PSSDas micelles (Fig. 5C). Significantly greater amounts of parent DAS were detected from cells treated with POEG-*b*-PSSDas as compared to cells treated with POEG-*b*-PCCDas, supporting the notion that the facilitated release of Das from POEG-*b*-PSSDas contributed significantly to the enhanced toxicity.

Fig. 6 shows the cytotoxicity of free DOX, DOX-loaded POEG-*b*-PCCDas and DOX-loaded POEG-*b*-PSSDas micelles in 4T1.2 (Fig. 6A) and PC3 cells (Fig. 6B). DOX-loaded POEG-*b*-PCCDas micelles were less effective in killing tumor cells than free DOX and DOX-loaded POEG-*b*-PSSDas micelles. It is likely that DOX/POEG-*b*-PSSDas micelles become disassembled in response to intracellular GSH following uptake, resulting in enhanced release of encapsulated DOX, and therefore, improved cell killing effect compared to DOX/POEG-*b*-PCCDas micelles. Table S2 shows the IC_{50} of free DOX, carrier alone and DOX-loaded micelles. The IC_{50} of DOX-loaded POEG-*b*-PSSDas micelles was 0.18 μg/mL in 4T1.2 cells, which was significantly lower than that of free DOX (IC_{50} = 0.45 μg/mL) and POEG-*b*-PSSDas prodrug carrier alone (IC_{50} = 1.49 μg/mL). Similar results were also found in PC3 cells, suggesting a synergistic effect between POEG-*b*-PSSDas carrier and the co-delivered DOX.

3.4. Intracellular trafficking and endocytosis mechanism

Intracellular distribution of DOX-loaded POEG-*b*-PCCDas and POEG-*b*-PSSDas micelles was investigated by confocal laser scanning microscopy (CLSM). 4T1.2 cells were incubated with free DOX, DOX/POEG-*b*-PCCDas and DOX/POEG-*b*-PSSDas micelles for 2 h and 6 h, respectively. At 2 h, for all the treatment groups, DOX fluorescence signals were found to be distributed largely in perinuclear region of cells, some of which were colocalized with endo/lysosomes (Fig. 7A). After 6 h incubation, compared with DOX/POEG-*b*-PCCDas, more DOX fluorescence signals appeared in nuclei for DOX/POEG-*b*-PSSDas micelles, which was comparable to that of free DOX (Fig. 7B). This result further indicated that introduction of disulfide linkage in the DOX/POEG-*b*-PSSDas system led to GSH-triggered micelle disassembly and rapid DOX release, which likely explains the higher cytotoxicity of DOX/POEG-*b*-PSSDas micelles over DOX/POEG-*b*-PCCDas micelles.

Endocytosis pathways of DOX/POEG-*b*-PSSDas and DOX/POEG-*b*-PCCDas micelles were then investigated by flow cytometry with different endocytosis inhibitors, including methyl-β-cyclodextrin (MBCD, caveolae-mediated endocytosis inhibitor), sucrose (clathrin-mediated endocytosis inhibitor) and cytochalasin D (macropinocytosis inhibitor) [42]. Fig. S6 shows the DOX fluorescence intensity in 4T1.2 cells after 2 h incubation with DOX/POEG-*b*-PSSDas micelles (Fig. S8A) or DOX/POEG-*b*-PCCDas micelles (Fig. S6B). DOX/POEG-*b*-PCCDas and

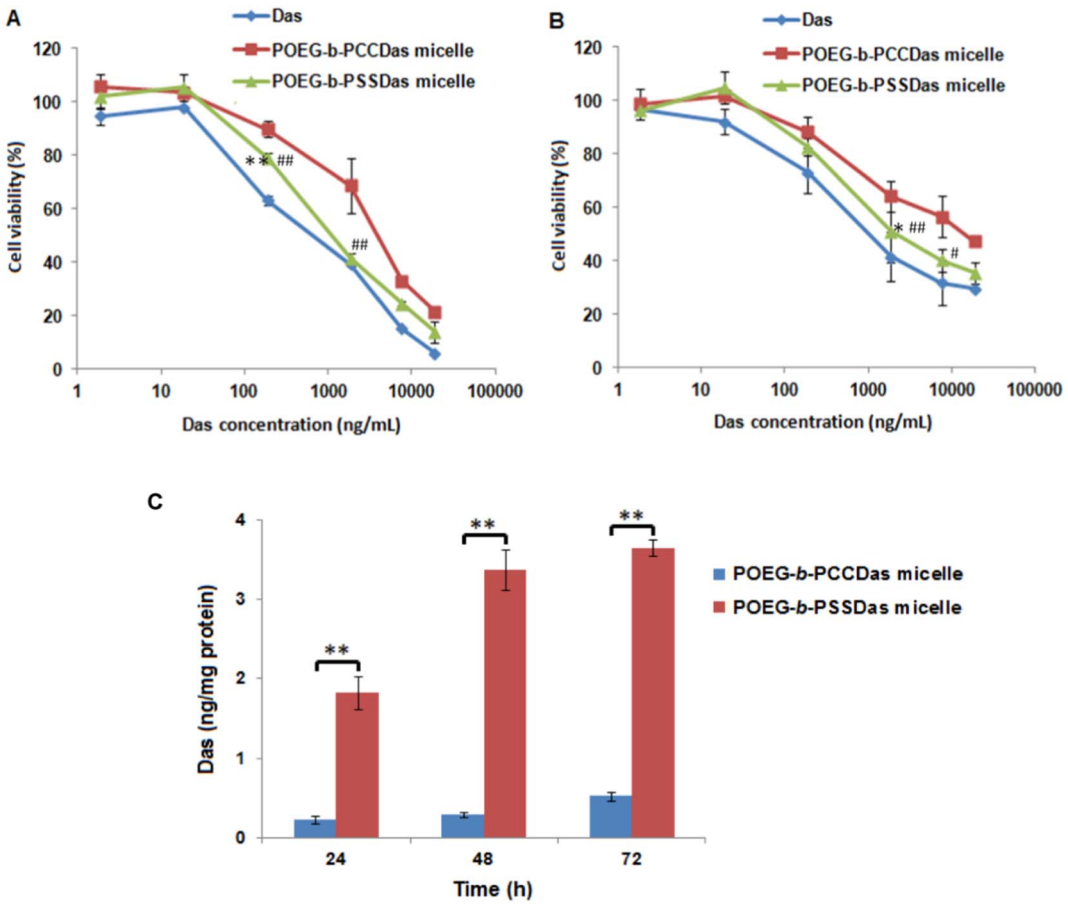

Fig. 5. MTT cytotoxicity of POEG-*b*-PCCDas and POEG-*b*-PSSDas prodrug micelles in 4T1.2 mouse breast cancer cell line (A) and PC3 human prostatic carcinoma cell line (B) with free DAS as the control. Cells were treated with different micelles for 72 h and values reported are the means ± SD for triplicate samples. *P < 0.05, **P < 0.01 (POEG-*b*-PSSDas micelles vs Das); $^{\#}$P < 0.05, $^{\#\#}$P < 0.01 (POEG-*b*-PSSDas micelles vs POEG-*b*-PCCDas micelles). (C) HPLC-MS analysis of the amounts of released free DAS in 4T1.2 cells treated with POEG-*b*-PCCDas and POEG-*b*-PSSDas micelles at different time points (24 h, 48 h, 72 h). **P < 0.01 (POEG-*b*-PSSDas micelle vs POEG-*b*-PCCDas micelle).

DOX/POEG-*b*-PSSDas were comparable in DOX uptake in the absence of endocytosis inhibitors, and the relative mean fluorescence intensity of both micelles were used as the reference (100%), respectively. Treatment with either inhibitor led to a significant decrease in the cellular uptake of DOX/POEG-*b*-PCCDas micelles with an inhibition rate of 86.7%, 80.4%, or 84.5% for MBCD, sucrose or cytochalasin D, respectively (Fig. S6A). These data suggest that DOX/POEG-*b*-PCCDas micelles were taken up by 4T1.2 cells via multiple pathways including macropinocytosis, clathrin-mediated endocytosis, and caveolae-mediated endocytosis, which are the three major endocytic pathways for macromolecules [42]. Similar results were shown for DOX/POEG-*b*-PSSDas micelles, suggesting that uptake of the two micellar carriers was mediated by similar mechanisms.

3.5. Plasma pharmacokinetics and tissue distribution

The plasma pharmacokinetic profiles of DOX/POEG-*b*-PCCDas and DOX/POEG-*b*-PSSDas micelles were evaluated with free DOX·HCl as a control. As shown in Fig. 8A, the plasma DOX concentrations decreased rapidly following i.v. administration of free DOX. In contrast, both DOX/POEG-*b*-PCCDas and DOX/POEG-*b*-PSSDas micelles showed a significantly slower kinetics of DOX clearance from the blood. The DOX concentrations for DOX/POEG-*b*-PCCDas and DOX/POEG-*b*-PSSDas were significantly higher than those for free DOX at all time

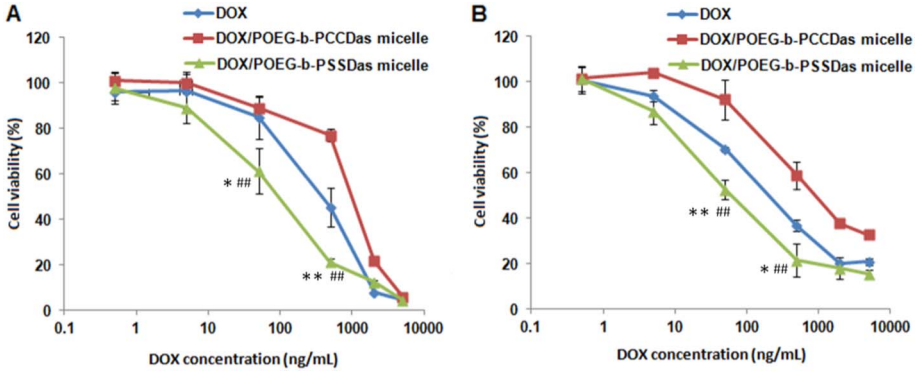

Fig. 6. MTT cytotoxicity assay of DOX-loaded POEG-*b*-PCCDas and POEG-*b*-PSSDas micelles in 4T1.2 (A) and PC3 cell line (B) after 72 h treatment. Data are presented as the means ± SD for triplicate samples.*P < 0.05, **P < 0.01 (DOX/POEG-*b*-PSSDas micelles vs Das); $^{\#\#}$P < 0.01 (DOX/POEG-*b*-PSSDas micelles vs POEG-*b*-PCCDas micelles).

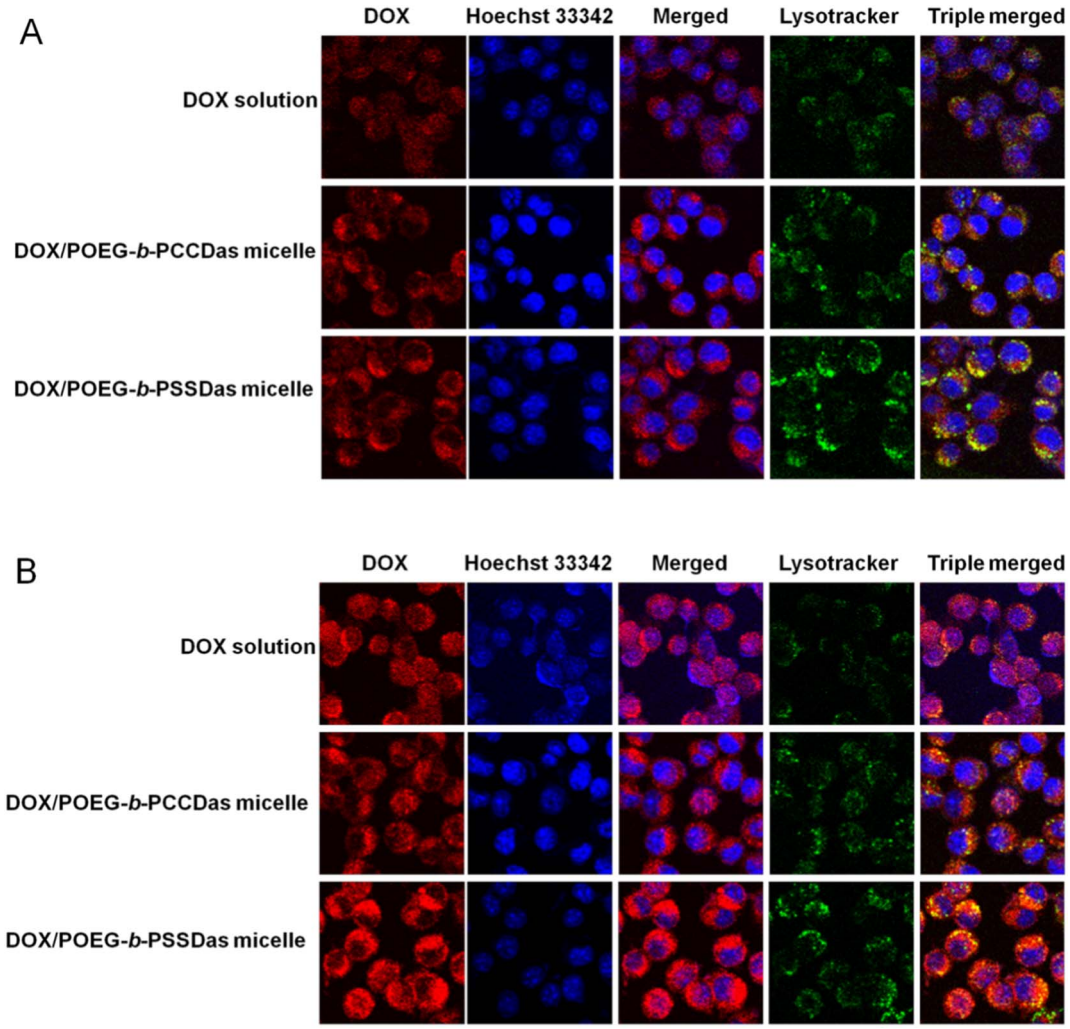

Fig. 7. Confocal laser scanning microscopic images of 4T1.2 cells after incubation with free DOX, DOX/POEG-*b*-PCCDas and DOX/POEG-*b*-PSSDas micelles for 2 h (A) and 6 h (B). The nuclei were stained with Hoechst 33342, and endo/lysosomes were stained by LysoTracker DND-26.

points examined. No significant difference was noticed between DOX/POEG-*b*-PCCDas and DOX/POEG-*b*-PSSDas in the kinetics of DOX clearance from the blood.

The tissue distribution of DOX for DOX/POEG-*b*-PCCDas and DOX/POEG-*b*-PSSDas micelles was also investigated in 4T1.2 tumor-bearing mice. Compared with free DOX, significantly higher amounts of DOX were detected in tumors after treatment with DOX/POEG-*b*-PCCDas or DOX/POEG-*b*-PSSDas micelles (Fig. 8B). In addition, tumors treated with DOX/POEG-*b*-PSSDas seemed to have more DOX accumulation compared to DOX/POEG-*b*-PCCDas group although it is not statistically

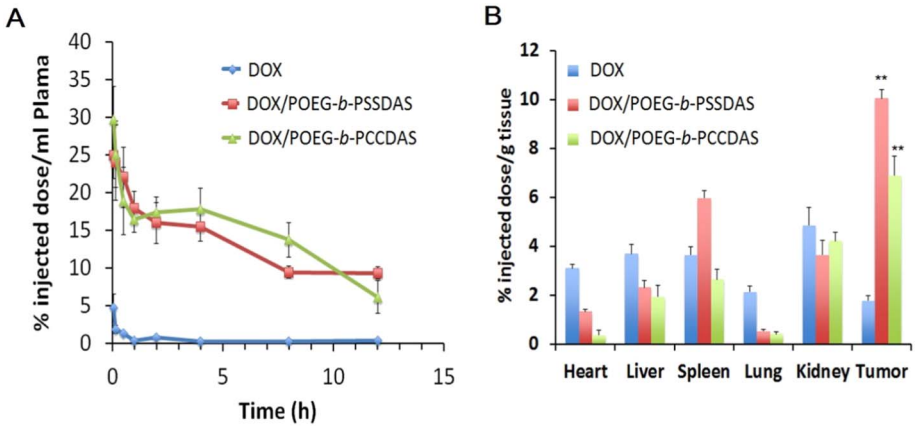

Fig. 8. Pharmacokinetics and biodistribution of DOX/POEG-*b*-PCCDas and DOX/POEG-*b*-PSSDas micelles. (A) Blood kinetics of DOX in CD-1 mice following i.v. injection of DOX/POEG-*b*-PCCDas and DOX/POEG-*b*-PSSDas micelles at a dose of 5 mg DOX/kg with free DOX as a control. (B) Tissue distribution of DOX in 4T1.2 tumor-bearing BALB/c mice 24 h following i.v. injection of DOX/POEG-*b*-PCCDas, DOX/POEG-*b*-PSSDas micelles or free DOX (5 mg DOX/kg). $^{**}P < 0.01$ (DOX/POEG-*b*-PSSDas micelle vs DOX, DOX/POEG-*b*-PCCDas micelle vs DOX).

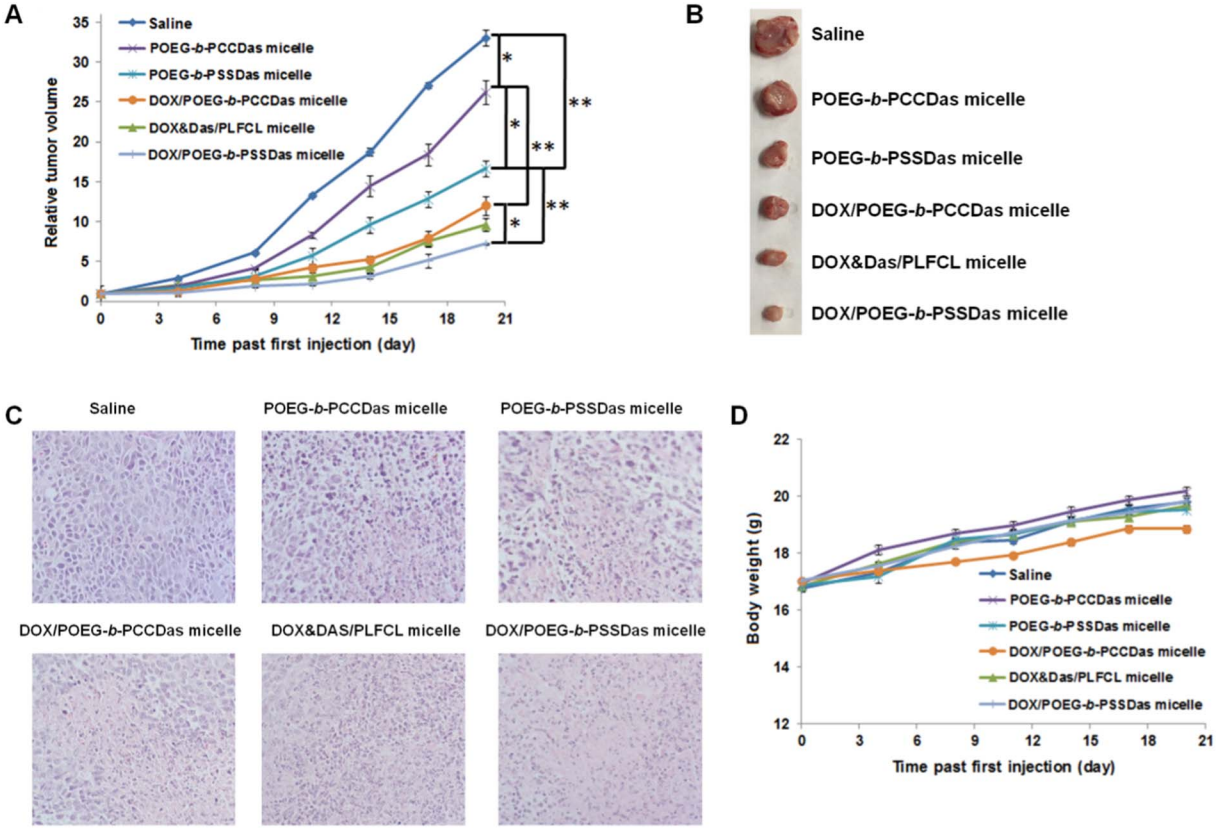

Fig. 9. In vivo antitumor activity of free and DOX-loaded POEG-*b*-PCCDas and POEG-*b*-PSSDas prodrug micelles in a syngeneic murine breast cancer model (4T1.2) with saline and DOX & DAS/PEG-Fmoc formulation as controls. Three injections on days 0, 4 and 8 were made with a DOX dosage of 5 mg/kg. (A) Tumor volume changes with time. Data are presented as mean ± SD (n = 8). *P < 0.05; **P < 0.01. (B) Representative photographs of the harvested tumor from each treatment group at day 20; (C) Histological analyses of tumor tissues collected on day 20 using H & E staining. (D) Changes of body weight in mice following different treatments.

significant (P = 0.13). More studies are required in the future to further confirm this difference. It is also apparent that DOX/POEG-*b*-PCCDas and DOX/POEG-*b*-PSSDas micelles showed more accumulation of DOX in tumors than in other tissues (Fig. 8B). These data demonstrated that POEG-*b*-PCCDas and POEG-*b*-PSSDas could serve as excellent carriers to efficiently deliver DOX into tumors.

We also performed a preliminary study in determining the amounts of free DAS in tumor tissues at 24 h following treatment with DOX/POEG-*b*-PCCDas and DOX/POEG-*b*-PSSDas micelles (Fig. S7). Significantly more DAS was found in tumors treated with DOX/POEG-*b*-PSSDas micelles compared to those treated with DOX/POEG-*b*-PCCDas. The differences in the amounts of free DAS between the two groups were much more dramatic than those in the amounts of DOX in the tumor tissues (Fig. 8B). This is likely due to a rapid release of DAS from POEG-*b*-PSSDas micelles after they reach the highly redox environment of tumors (Fig. 4A). It is hypothesized that DAS is released from POEG-*b*-PCCDas through the enzyme-mediated hydrolysis, which is relatively ineffective due to the steric hindrance of POEG hydrophilic shell. This will be different for POEG-*b*-PSSDas micelles in which the disulfide linkage is first cleaved in response to the high GSH levels in tumor cells. The released small DAS-conjugates are then effectively hydrolyzed by the intracellular esterases to generate the parent DAS (Fig. S8). Of course, a likely more effective uptake of DOX/POEG-*b*-PSSDas micelles by tumors might also contribute to the more free DAS detected in tumor tissues. More studies are needed in the future to further confirm this hypothesis. Nevertheless, these results suggested that introduction of disulfide linkage into the POEG-*b*-PSSDas led to higher effective concentrations of DAS in tumor tissues, which shall play an important role in improving the anti-tumor activity of the prodrug carrier.

3.6. *In vivo therapeutic efficacy*

The in vivo therapeutic efficacy of POEG-*b*-PSSDas prodrug carrier and DOX/POEG-*b*-PSSDas mixed micelles was evaluated in an aggressive 4T1.2 mouse tumor model. Previously, our group developed a pharmacologically "inert" PEG-peptidic conjugate (PLFCL) as a carrier for codelivery of DOX and DAS, and discovered that DOX & DAS/PLFCL micelles were much more effective in tumor inhibition than the free DOX and DAS combination [31]. So DOX & DAS/PLFCL micelles were also included as a control in this study. As shown in Fig. 8A, POEG-*b*-PSSDas prodrug micelles showed much better anti-tumor activity than POEG-*b*-PCCDas micelles (*P < 0.05), which was consistent with the in vitro MTT cytotoxicity results (Fig. 5). It is also noted that both POEG-*b*-PCCDas and POEG-*b*-PSSDas micelles exhibited significantly improved therapeutic effect after loading DOX (**P < 0.01), suggesting that the DAS cleaved from the prodrug carriers could produce synergistic antitumor effect with co-delivered DOX. Moreover, DOX-loaded POEG-*b*-PSSDas micelles were more active than DOX-loaded POEG-*b*-PCCDas micelles in inhibiting tumor growth, further confirming that incorporation of disulfide linkage into the polymer systems resulted in an overall improvement in tumor-inhibition effect either for prodrug alone or DOX-loaded micelles.

Fig. 9A also shows that DOX-loaded POEG-*b*-PSSDas micelles were more effective than PLFCL micelles co-loaded with DOX and DAS at the same dose of DOX and DAS, which suggested that the DAS-based prodrug carrier strategy was more suitable for co-delivery of DAS and DOX. The possible reason is that the nature of DAS makes it difficult to be encapsulated by micelles and the noncovalent encapsulation of DAS and DOX into one single micellar system will result in poor stability in vivo, leading to premature DAS release before being delivered to tumor sites. In contrast, DAS-conjugated prodrug strategy can effectively

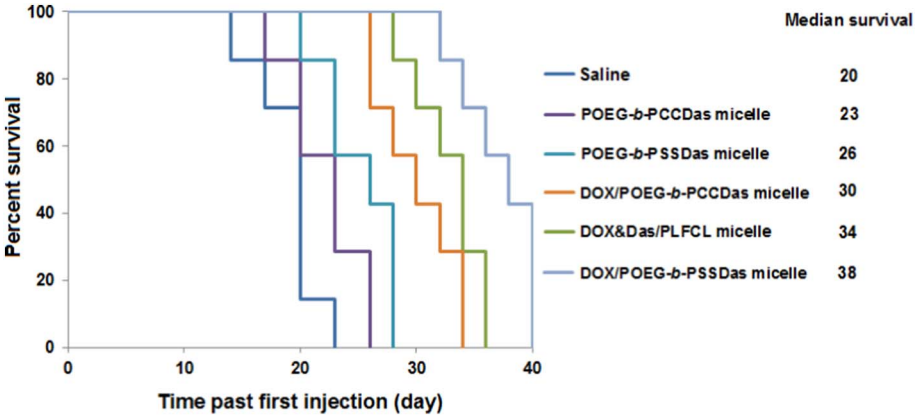

Fig. 10. Kaplan-Meier survival curves for syngeneic murine breast cancer model (4T1.2) after various treatments. Three injections were made on days 0, 4 and 8.

prevent premature DAS release in the blood circulation and promote drug release at the tumor sites to maximally exert its antitumor activity.

Fig. 9B showed the photographs of the harvested tumors on day 20. The smallest tumor size was observed for the mice treated with DOX-loaded POEG-*b*-PSSDas micelles, which further confirmed its improved therapeutic efficacy over other formulations. Then, the histological changes of tumors following different treatments were analyzed by H & E staining. As shown in Fig. 9C, the tumors in saline-treated mice showed typical morphology of cancer cells with large nuclei. The tumor tissues in other treatment groups showed altered morphology with cell damage and shrunk nuclei. The group treated with DOX-loaded POEG-*b*-PSSDas micelles exhibited the largest necrosis area, further validating the best anti-tumor activity of this redox-responsive combination therapy. All of the treatments were well-tolerated as demonstrated by similar increases in body weighs over time compared to control group (Fig. 9D).

In a separate experiment, the survival rates of the mice with different treatments were further examined. As shown in Fig. 10, control mice group treated with saline exhibited a short median survival time of 20 days. In comparison, mice treated with POEG-*b*-PCCDas, POEG-*b*-PSSDas, DOX/POEG-*b*-PCCDas, and DOX & DAS/PLFCL had an improved survival rate with a median survival time of 23, 26, 30, and 34 days, respectively. The longest survival time (38 days) was observed in the group treated with DOX-loaded POEG-*b*-PSSDas micelles, which suggested that incorporation of disulfide linkage into the prodrug system could not only suppress the tumor growth, but also prolong the survival time. These results clearly demonstrate that the combination of chemotherapy and targeted therapy achieved by our redox-responsive DOX/POEG-*b*-PSSDas micelles leads to an improved and synergistic therapeutic effect, which warrants further investigation.

4. Conclusions

We have developed a redox-sensitive, polymeric prodrug carrier, POEG-*b*-PSSDas for effective co-delivery of DAS and DOX. Compared to a redox-insensitive counterpart, POEG-*b*-PCCDas, POEG-*b*-PSSDas was more active either as carrier alone or as DOX/carrier mixed micelles, which is likely attributed to the accelerated release of both DAS and DOX following intracellular delivery. More importantly, in vivo delivery of DOX via POEG-*b*-PSSDas prodrug carrier led to significant inhibition of tumor growth, which was more effective than codelivery of DAS and DOX via a pharmacologically “inert” micellar carrier.

Acknowledgments

This work was supported by NIH grants no. RO1CA173887, no. R01GM102989, no. R01HL083365, and no. R21CA173887.

Appendix A. Supplementary data

Supplementary data to this article can be found online at http://dx.doi.org/10.1016/j.jconrel.2017.05.006.

References

[1] L. Ma, M. Kohli, A. Smith, Nanoparticles for combination drug therapy, ACS Nano 7 (2013) 9518–9525.
[2] N. Kolishetti, S. Dhar, P.M. Valencia, L.Q. Lin, R. Karnik, S.J. Lippard, R. Langer, O.C. Farokhzad, Engineering of self-assembled nanoparticle platform for precisely controlled combination drug therapy, Proc. Natl. Acad. Sci. U. S. A. 107 (2010) 17939–17944.
[3] D. Lane, Designer combination therapy for cancer, Nat. Biotechnol. 24 (2006) 163–164.
[4] A. Jhaveri, P. Deshpande, V. Torchilin, Stimuli-sensitive nanopreparations for combination cancer therapy, J. Control. Release 190 (2014) 352–370.
[5] J. Zhang, P.L. Yang, N.S. Gray, Targeting cancer with small molecule kinase inhibitors, Nat. Rev. Cancer 9 (2009) 28–39.
[6] M. Maemondo, A. Inoue, K. Kobayashi, S. Sugawara, S. Oizumi, H. Isobe, A. Gemma, M. Harada, H. Yoshizawa, I. Kinoshita, Gefitinib or chemotherapy for non-small-cell lung cancer with mutated EGFR, N. Engl. J. Med. 362 (2010) 2380–2388.
[7] J. Xiao, M. Xu, T. Hou, Y. Huang, C. Yang, J. Li, Dasatinib enhances antitumor activity of paclitaxel in ovarian cancer through Src signaling, Mol. Med. Rep. 12 (2015) 3249–3256.
[8] H. Kantarjian, N.P. Shah, A. Hochhaus, J. Cortes, S. Shah, M. Ayala, B. Moiraghi, Z. Shen, J. Mayer, R. Pasquini, Dasatinib versus imatinib in newly diagnosed chronic-phase chronic myeloid leukemia, New Engl. J. Med. 362 (2010) 2260–2270.
[9] L. Rice, S. Lepler, C. Pampo, D.W. Siemann, Impact of the SRC inhibitor dasatinib on the metastatic phenotype of human prostate cancer cells, Clin. Exp. Metastasis 29 (2012) 133–142.
[10] E. Weisberg, P.W. Manley, S.W. Cowan-Jacob, A. Hochhaus, J.D. Griffin, Second generation inhibitors of BCR-ABL for the treatment of imatinib-resistant chronic myeloid leukaemia, Nat. Rev. Cancer 7 (2007) 345–356.
[11] P. Ceppi, M. Papotti, V. Monica, M.L. Iacono, S. Saviozzi, M. Pautasso, S. Novello, S. Mussino, E. Bracco, M. Volante, Effects of Src kinase inhibition induced by dasatinib in non–small cell lung cancer cell lines treated with cisplatin, Mol. Cancer Ther. 8 (2009) 3066–3074.
[12] S. Nam, D. Kim, J.Q. Cheng, S. Zhang, J.-H. Lee, R. Buettner, J. Mirosevich, F.Y. Lee, R. Jove, Action of the Src family kinase inhibitor, dasatinib (BMS-354825), on human prostate cancer cells, Cancer Res. 65 (2005) 9185–9189.
[13] G. Konecny, R. Glas, J. Dering, K. Manivong, J. Qi, R. Finn, G. Yang, K. Hong, C. Ginther, B. Winterhoff, Activity of the multikinase inhibitor dasatinib against ovarian cancer cells, Br. J. Cancer 101 (2009) 1699–1708.
[14] L.J. Lombardo, F.Y. Lee, P. Chen, D. Norris, J.C. Barrish, K. Behnia, S. Castaneda, L.A. Cornelius, J. Das, A.M. Doweyko, Discovery of N-(2-chloro-6-methyl-phenyl)-2-(6-(4-(2-hydroxyethyl)-piperazin-1-yl)-2-methylpyrimidin-4-ylamino) thiazole-5-carboxamide (BMS-354825), a dual Src/Abl kinase inhibitor with potent antitumor activity in preclinical assays, J. Med. Chem. 47 (2004) 6658–6661.
[15] N.P. Shah, C. Tran, F.Y. Lee, P. Chen, D. Norris, C.L. Sawyers, Overriding imatinib resistance with a novel ABL kinase inhibitor, Science 305 (2004) 399–401.
[16] E.M. Kim, K. Mueller, E. Gartner, J. Boerner, Dasatinib is synergistic with cetuximab and cisplatin in triple-negative breast cancer cells, J. Surg. Res. 185 (2013) 231–239.
[17] A.A. Secord, D.K. Teoh, W.T. Barry, M. Yu, G. Broadwater, L.J. Havrilesky, P.S. Lee, A. Berchuck, J. Lancaster, R.M. Wenham, A phase I trial of dasatinib, an SRC-family kinase inhibitor, in combination with paclitaxel and carboplatin in patients with advanced or recurrent ovarian cancer, Clin. Cancer Res. 18 (2012) 5489–5498.
[18] D. Teoh, T.A. Ayeni, J.M. Rubatt, D.J. Adams, L. Grace, M.D. Starr, W.T. Barry,

A. Berchuck, S.K. Murphy, A.A. Secord, Dasatinib (BMS-35482) has synergistic activity with paclitaxel and carboplatin in ovarian cancer cells, Gynecol. Oncol. 121 (2011) 187–192.
[19] B.J. Park, Z.L. Whichard, S.J. Corey, Dasatinib synergizes with both cytotoxic and signal transduction inhibitors in heterogeneous breast cancer cell lines–lessons for design of combination targeted therapy, Cancer Lett. 320 (2012) 104–110.
[20] T. Chen, C. Wang, Q. Liu, Q. Meng, H. Sun, X. Huo, P. Sun, J. Peng, Z. Liu, X. Yang, Dasatinib reverses the multidrug resistance of breast cancer MCF-7 cells to doxorubicin by downregulating P-gp expression via inhibiting the activation of ERK signaling pathway, Cancer Biol. Ther. 16 (2015) 106–114.
[21] C. Pichot, S. Hartig, L. Xia, C. Arvanitis, D. Monisvais, F. Lee, J. Frost, S. Corey, Dasatinib synergizes with doxorubicin to block growth, migration, and invasion of breast cancer cells, Br. J. Cancer 101 (2009) 38–47.
[22] J. Van Oosterwijk, M. van Ruler, I. Briaire-de Bruijn, B. Herpers, H. Gelderblom, B. van de Water, J. Bovée, Src kinases in chondrosarcoma chemoresistance and migration: dasatinib sensitises to doxorubicin in TP53 mutant cells, Br. J. Cancer 109 (2013) 1214–1222.
[23] L.D. Mayer, T.O. Harasym, P.G. Tardi, N.L. Harasym, C.R. Shew, S.A. Johnstone, E.C. Ramsay, M.B. Bally, A.S. Janoff, Ratiometric dosing of anticancer drug combinations: controlling drug ratios after systemic administration regulates therapeutic activity in tumor-bearing mice, Mol. Cancer Ther. 5 (2006) 1854–1863.
[24] C. Poon, C. He, D. Liu, K. Lu, W. Lin, Self-assembled nanoscale coordination polymers carrying oxaliplatin and gemcitabine for synergistic combination therapy of pancreatic cancer, J. Control. Release 201 (2015) 90–99.
[25] M. Huo, J. Yuan, L. Tao, Y. Wei, Redox-responsive polymers for drug delivery: from molecular design to applications, Polym. Chem. 5 (2014) 1519–1528.
[26] J. Sun, R. Sheng, T. Luo, Z. Wang, H. Li, A. Cao, Synthesis of diblock/statistical cationic glycopolymers with pendant galactose and lysine moieties: gene delivery application and intracellular behaviors, J. Mater. Chem. B (2016) 4696–4706.
[27] H. Wei, R.-X. Zhuo, X.-Z. Zhang, Design and development of polymeric micelles with cleavable links for intracellular drug delivery, Prog. Polym. Sci. 38 (2013) 503–535.
[28] J. Sun, T. Luo, R. Sheng, H. Li, S. Chen, F. Hu, A. Cao, Preparation of functional water-soluble low-cytotoxic poly(methacrylate)s with pendant cationic l-lysines for efficient gene delivery, Macromol. Biosci. 13 (2013) 35–47.
[29] H. Maeda, H. Nakamura, J. Fang, The EPR effect for macromolecular drug delivery to solid tumors: improvement of tumor uptake, lowering of systemic toxicity, and distinct tumor imaging in vivo, Adv. Drug Deliv. Rev. 65 (2013) 71–79.
[30] Q. Li, K.L. Lai, P.S. Chan, S.C. Leung, H.Y. Li, Y. Fang, K.K. To, C.H.J. Choi, Q.Y. Gao, T.W. Lee, Micellar delivery of dasatinib for the inhibition of pathologic cellular processes of the retinal pigment epithelium, Colloids Surf. B 140 (2016) 278–286.
[31] P. Zhang, J. Li, M. Ghazwani, W. Zhao, Y. Huang, X. Zhang, R. Venkataramanan, S. Li, Effective co-delivery of doxorubicin and dasatinib using a PEG-Fmoc nanocarrier for combination cancer chemotherapy, Biomaterials 67 (2015) 104–114.
[32] R. Duncan, The dawning era of polymer therapeutics, Nat. Rev. Drug Discov. 2 (2003) 347–360.
[33] H. Son, S. Srinivasan, J. Yhee, D. Das, B. Daugherty, G. Berguig, V. Oehle, S. Kim, K. Kim, I. Kwon, Chemotherapeutic copolymers prepared via the RAFT polymerization of prodrug monomers, Polym. Chem. 7 (2016) 4494–4505.
[34] J. Sun, Y. Chen, K. Li, Y. Huang, X. Fu, X. Zhang, W. Zhao, Y. Wei, L. Xu, P. Zhang, A prodrug micellar carrier assembled from polymers with pendant farnesyl thiosalicylic acid moieties for improved delivery of paclitaxel, Acta Biomater. 43 (2016) 282–291.
[35] R. Cheng, F. Meng, C. Deng, H.-A. Klok, Z. Zhong, Dual and multi-stimuli responsive polymeric nanoparticles for programmed site-specific drug delivery, Biomaterials 34 (2013) 3647–3657.
[36] Y. Bao, Y. Guo, X. Zhuang, D. Li, B. Cheng, S. Tan, Z. Zhang, D-α-tocopherol polyethylene glycol succinate-based redox-sensitive paclitaxel prodrug for overcoming multidrug resistance in cancer cells, Mol. Pharm. 11 (2014) 3196–3209.
[37] F. Meng, W.E. Hennink, Z. Zhong, Reduction-sensitive polymers and bioconjugates for biomedical applications, Biomaterials 30 (2009) 2180–2198.
[38] X. Zhang, K. Liu, Y. Huang, J. Xu, J. Li, X. Ma, S. Li, Reduction-sensitive dual functional nanomicelles for improved delivery of paclitaxel, Bioconjug. Chem. 25 (2014) 1689–1696.
[39] H. Li, T. Luo, R. Sheng, J. Sun, Z. Wang, A. Cao, Endoplasmic reticulum localization of poly (ω-aminohexyl methacrylamide) s conjugated with (l-)-arginines in plasmid DNA delivery, Biomaterials 34 (2013) 7923–7938.
[40] P. Sun, D. Zhou, Z. Gan, Novel reduction-sensitive micelles for triggered intracellular drug release, J. Control. Release 155 (2011) 96–103.
[41] R.E. Wang, T. Liu, Y. Wang, Y. Cao, J. Du, X. Luo, V. Deshmukh, C.H. Kim, B.R. Lawson, M.S. Tremblay, An immunosuppressive antibody-drug conjugate, J. Am. Chem. Soc. 137 (2015) 3229–3232.
[42] C. Cui, Y.-N. Xue, M. Wu, Y. Zhang, P. Yu, L. Liu, R.-X. Zhuo, S.-W. Huang, Cellular uptake, intracellular trafficking, and antitumor efficacy of doxorubicin-loaded reduction-sensitive micelles, Biomaterials 34 (2013) 3858–3869.
[43] S. Petersen, S. Barcikowski, In situ bioconjugation: single step approach to tailored nanoparticle-bioconjugates by ultrashort pulsed laser ablation, Adv. Funct. Mater. 19 (2009) 1167–1172.
[44] D. Tan, S. Zhou, B. Xu, P. Chen, Y. Shimotsuma, K. Miura, J. Qiu, Simple synthesis of ultra-small nanodiamonds with tunable size and photoluminescence, Carbon 62 (2013) 374–381.
[45] P. Wagener, A. Schwenke, B.N. Chichkov, S. Barcikowski, Pulsed laser ablation of zinc in tetrahydrofuran: bypassing the cavitation bubble, J. Phys. Chem. C 114 (2010) 7618–7625.